PERGAMON

International Journal of Heat and Mass Transfer 42 (1999) 2811–2822

International Journal of HEAT and MASS TRANSFER

Stability of thermally driven shear flows in long inclined cavities with end-to-end temperature difference

R. Delgado-Buscalioni*, E. Crespo del Arco

Departamento de Física Fundamental, Universidad de Educación a Distancia, Senda del Rey s/n, E-28040, Madrid, Spain

Received 16 October 1997; in final form 25 October 1998

Abstract

The stability of buoyancy driven shear flows in inclined long cavities with end wall temperature difference is investigated for different inclinations and a wide range of Prandtl number. The results of the linear stability analysis show that the basic unicellular motion may break down due to stationary or oscillatory instabilities. The stationary rolls are nearly square and the mechanism of this instability is mainly hydrodynamic. The oscillatory instability is driven by buoyancy and consists of long-wave rolls of about 10 times the width of the cavity. For $Pr < 0.2$ stationary modes are the most unstable while for $Pr > 0.7$ oscillatory modes are preferred. At moderate Prandtl numbers ($0.2 < Pr < 0.7$) the most unstable perturbation is determined by the angle of inclination. A better understanding of the instability mechanisms is provided by an energy analysis of the marginally stable perturbations.

Results from direct numerical simulations of the full non-linear unsteady equations in closed configurations are also presented. Both stationary and oscillatory instabilities have been obtained and their characteristic features (wave number and frequency) are consistent with the linear theoretical predictions.

Nomenclature

c phase velocity of critical perturbations
$\mathbf{g}$ gravity vector
h half width of the cavity
k real wave number
L length of the cavity
N number of basis functions
p dimensionless pressure
Pr Prandtl number
R Rayleigh number
T dimensionless temperature
$\mathbf{v}$ velocity vector
u, w velocities in the x and z direction respectively
$w_{\max}(z)$ is the maximum upslope velocity along x at the core region
x, z coordinates.

Greek symbols
α inclination angle
β thermal expansion coefficient
ΔT temperature difference between end walls
$\varepsilon = 2h/L$ aspect ratio
κ thermal diffusivity
λ complex growth rate of perturbations
ν kinematic viscosity
η dimensionless temperature gradient along z in the core region
Ψ perturbation streamfunction
Θ perturbation temperature
φ, θ amplitudes of the stream function and temperature perturbations
ω angular frequency.

Subscripts
c critical value
o basic state
os oscillatory
st stationary.

1. Introduction

Natural convection in shallow cavities driven by an end-to-end temperature difference have received an

* Corresponding author.

0017–9310/99/$ - see front matter
PII: S0017–9310(98)00352–4

increasing attention since the last decade due to its relevance in several technological and fundamental areas. Most part of the published works on this subject consider cavities placed horizontally [1]. Convection in long inclined cavities driven by a temperature gradient along their longest axis is also important for a variety of phenomena that occur in industry and in nature. For instance, in crystal growth from vapor phase, larger transport rates are obtained by tilting the ampoule a certain angle with respect to gravity [2, 3]. Natural convection in tilted fluid layers is also found in many geophysical situations where the fluid is enclosed in long narrow slots arbitrarily inclined to gravity [4, 5]. An interesting application is the transport and rate of spread of passive contaminants (for instance, radioactive material) in long tilted liquid-filled rock fractures. Woods and Lintz [4] studied this problem and concluded that the contribution of the base flow to the transport rate is larger than that of diffusion. Though they did not consider the secondary flow, they assess its importance in modifying the overall mass flux. In this paper we investigate the basic and secondary flow in an inclined cavity as indicated in the geometry of the problem shown in Fig. 1.

Two particular limit cases of the geometry of Fig. 1 correspond to vertical cavities heated from below, $\alpha = 0^\circ$, and horizontal cavities with lateral heating, $\alpha = 90^\circ$. For $\alpha = 0^\circ$, the basic state is purely conductive (rest solution). Stability analysis of the rest solution was studied by Gershuni and Zhukhovitskii [6]; the critical Rayleigh number corresponds to odd perturbations with infinite wavelength. In the horizontal case, $\alpha = 90^\circ$, a basic circulation arises for any small non-zero temperature gradient. This case was first comprehensively studied in the series of papers by Cormack et al. [7] and Imberger [8] and, since then, it has been extensively revised (see Ref. [1]). The linear stability analysis of the parallel flow solution for $\alpha = 90^\circ$, was first carried out by Hart [9] and revised by Laure and Roux [10] and Kuo and Korpela [11]. These works considered the marginal stability of longitudinal

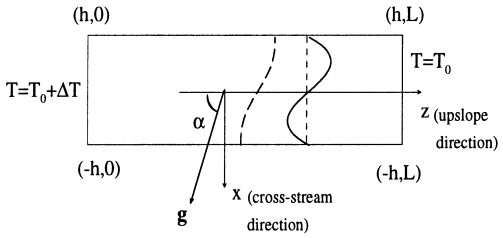

Fig. 1. Geometry of the problem and structure of the basic flow. Solid line represents the basic velocity profile and dashed line the temperature profile.

(three-dimensional) and transversal (two-dimensional) perturbations in low Pr fluids. Janssen and Henkes [12] studied numerically the steady and time-dependent two-dimensional flow in a horizontal square cavity and also the effect of a third direction (depth) on the instabilities [13]. They showed that for depth-to-width ratio $D/2h \geqslant 0.2$, the steady flow is in good approximation two-dimensional in the central region of the three-dimensional cavity. For $D/2h \geqslant 1$ they observed a wave-like stationary modulation along the depth superposed to the two-dimensional flow. For $D/2h = 0.5$ this longitudinal instability was not found and in this case, the observed critical instability was two-dimensional.

In the inclined cavity of Fig. 1, the basic flow arises for any temperature difference and its intensity increases steeply with the Rayleigh number as long as the isotherms are distorted by advection. The type of flow that arises is similar to that described by Woods and Lintz [4] in inclined liquid-filled rock fractures with vertical thermal gradient. In particular, the shape of our flow coincides to that described in Ref. [4] in their limit of vanishing ratio between rock and liquid thermal conductivities. Adachi and Mizushima [14] studied the stability of thermal convection in a similar inclined geometry in a square two-dimensional cavity. Bontoux et al. [3] considered the steady flow in long inclined axially heated cylinders and showed that for large enough Rayleigh number, the structure of the three dimensional flow is very similar to the flow observed in vertical cylinders after the onset of convection [15].

Although the effect of inclined boundaries on the flow stability has been treated in a variety of geometries (see Ref. [6] for a classical review), as far as we know, there are no published works considering the stability of the base flow in long inclined cavities with axial temperature gradient. Among the studies which considered inclined walls, the natural convection between differentially heated inclined plates [16], is an interesting example of how the inclination determines the interplay between convective and hydrodynamical instability mechanism.

This paper considers the stability of thermally driven shear flows in axially heated inclined long cavities. The breakdown of the unicellular flow may be due to stationary or oscillatory instabilities depending mostly on the Prandtl number and also on the inclination angle. In Section 2, we obtain and discuss the basic flow solution in closed cavities. The stability analysis of the basic flow to perturbations periodic in the axial direction is considered in Section 3. In Section 4 the energy balance for the marginally stable solutions is presented. The results are reported in Section 5, and discussed in Section 6 where the stability boundaries in the parameter space (Pr, α) are also presented. Numerical solutions of the nonlinear flow in Section 7, assess the stability results and provide information on the flow at supercritical Rayleigh number. Some concluding remarks are given in Section 8.

2. Governing equations and basic flow

Let us consider the flow in the two dimensional cavity of Fig. 1. The cavity is filled with an incompressible fluid and inclined α degrees with respect to gravity. Owing to the existence of a temperature difference between the end walls a convective motion is established. The equations governing the motion are the Navier-Stokes and heat transport equations with the Boussinesq approximation. By using, h^2/v, h, v/h, $\Delta T\, h/L$ as scales for time, length, velocity and temperature respectively, the dimensionless equations are:

$$\nabla\cdot\mathbf{v}=0,$$

$$\partial\mathbf{v}/\partial t+(\mathbf{v}\cdot\nabla)\mathbf{v}=-\nabla p+\Delta\mathbf{v}-RPr^{-1}T\mathbf{e}_g. \tag{1}$$

$$\partial T/\partial t+(v\cdot\nabla)T=Pr^{-1}\Delta T, \tag{2}$$

where $\mathbf{e}_g=\sin\alpha\hat{\mathbf{i}}-\cos\alpha\hat{\mathbf{k}}$, is the gravity versor. The Rayleigh number and Prandtl number are defined respectively as $R=g\beta\Delta Th^4/v\kappa L$ and $Pr=v/\kappa$.

The non-slip condition is used at all rigid boundaries, and the temperature in the walls $x=\pm1$ satisfies the homogenous heat-conduction equation:

$$\mathbf{v}=0 \text{ at all boundaries} \tag{3}$$

$$\frac{\partial T}{\partial x}=0 \quad \text{at } x=\pm1 \tag{4}$$

As discussed in previous works Refs. [6 and 7] in the limit of vanishing ε, a simple exact parallel-flow solution exists in the core region, away from square turning region near the end walls. At the core, the velocity, $\mathbf{v}_o=u_o\hat{\mathbf{i}}+w_o\hat{\mathbf{k}}$ satisfies $u_o=0$, $w_o=w_o(x)$ and the temperature field is, $T_o(x,z)=-\eta z+b+\theta_o(x)$.

Substituting these solutions into equations (1) and (2), and eliminating p by cross differentiation, the following system of ordinary differential equations for $w_o(x)$ and $\theta_o(x)$ is obtained:

$$w_o'''(x)+Pr^{-1}R\cos\alpha\theta_o'(x)=\eta Pr^{-1}R\sin\alpha, \tag{5}$$

$$\eta w_o(x)+Pr^{-1}\theta_o''(x)=0. \tag{6}$$

with

$$w_o(\pm1)=\theta_o'(\pm1)=0. \tag{7}$$

Hereafter the primes denote differentiation with respect to x.

The solution of equations (5)–(7) is

$$w_o(x)=\frac{r\tan\alpha}{Pr}\left(\frac{\sin r\sinh rx-\sinh r\sin rx}{\mathrm{d}(r)}\right), \tag{8}$$

$$\theta_o(x)=-\eta\frac{\tan\alpha}{r}\left(\frac{\sin r\sinh rx+\sinh r\sin rx}{\mathrm{d}(r)}-rx\right), \tag{9}$$

where $\mathrm{d}(r)$ is

$$\mathrm{d}(r)=\sinh r\cos r+\cosh r\sin r, \tag{10}$$

and

$$r\equiv(\eta R\cos\alpha)^{1/4}. \tag{11}$$

For fixed α and Pr the amplitude of the basic flow is controlled by the group parameter $\eta R\cos\alpha$. The parallel flow solution describes a natural counterflow heat exchanger. The cooler current occupies the region $x>0$ and it is heated as it moves downwards in the $z-$axis. In the interval $0<r^4<R^*$, ($R^*=31.284$), an increase of r raises the amplitude of the basic core flow solutions and both w_o and θ_o become infinity as $r^4\to R^*$. For r^4 above R^* there is an inversion of the basic solutions and a new node appears. This fact occurs at each root of $\mathrm{d}(r)$ whose values, $r\approx(n-1/4)\pi$, $n=1,2,\ldots$ coincide with the fourth root of the critical Rayleigh number for the instability of even modes in the case of $\alpha=0^\circ$ [6].

The divergence of the basic profiles at certain values of r has been reported in other configurations which considered infinitely long cavities ($\varepsilon=0$) [4], [6]. We have found that in closed cavities (even in the limit $\varepsilon\to0$), $r^4<R^*$ for any R thus, the basic flow does not diverge. This is illustrated in Fig. 2 where numerical (see section 7) and theoretical calculations of the local Rayleigh number at the core ηR are plotted vs R. The theoretical calculation of η (in terms of R, α and ε) has been done by using the integral method proposed by Bejan and Tien [17]. At low R, the axial temperature gradient is constant along the cavity ($\eta\simeq1$) and the flow is mainly driven by the cross-stream buoyancy, proportional to $\eta R\sin\alpha$. This situation corresponds to a core driven regime [7, 8]. As R increases, the cross-stream temperature gradient created by the counterflow advection becomes larger and acts as another source of motion [related to the term

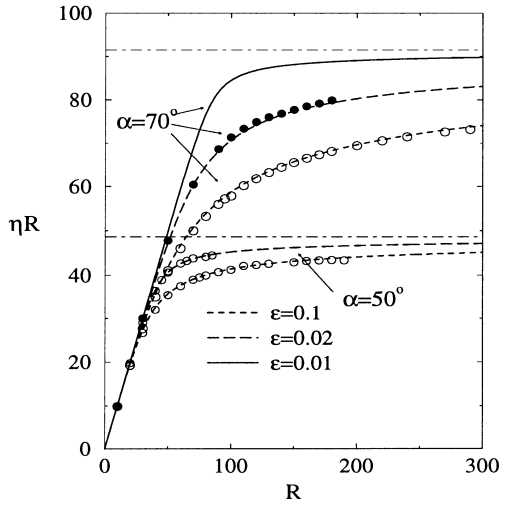

Fig. 2. The local Rayleigh at the core (ηR) vs external Rayleigh number (R) for several inclinations and aspect ratios. Solid lines correspond to the theoretical solution and circles are results from the numerical solution in the closed geometry (see section 7) using $Pr=0.7$ (white circles) and $Pr=6.7$ (black circles).

$R\cos\alpha\theta_o'$ in equation (5)]. This coupling of the velocity and temperature x-gradient induces a steep increase of the mean flow intensity as ηR approaches $R^*/\cos\alpha$ and leads to a boundary layer regime in which the temperature drop concentrates near the end regions ($\eta < 1$). As R further increases, ηR tends asymptotically to $R^*/\cos\alpha$ (see Fig. 2). This fact indicates that in inclined cavities (as long as the flow is unicellular), the local Rayleigh number at the core will not exceed a limit value, $R^*/\cos\alpha$.

3. Linear stability analysis

In this section we investigate the stability of the basic flow to infinitesimal perturbations periodic in the axial direction (z) and developed in the core of the cavity.

In the stability analysis of the core flow, it is preferable to use the local temperature z-gradient at the core, $\eta\Delta T/L$, in the temperature scaling. Hereafter (except in section 7, where we present numerical results in the closed geometry) the scale of temperature is $(\eta\Delta T/L)h$. By using this scale, $\partial T_o/\partial z = -1$; R corresponds to the local Rayleigh number at the core of the cavity and the basic velocity and temperature fields are those given in equations (8) and (9), with $\eta = 1$.

In order to study the stability of the basic flow we proceed in the usual form. The flow variables are written as the sum of the mean flow quantity and a small perturbation. The stream function of the perturbation flow satisfies

$$u = \frac{\partial\Psi}{\partial z}, \quad w = -\frac{\partial\Psi}{\partial x}.$$

We ascribe to the stream function and temperature perturbations, Θ, a dependence on z, t of the form

$$\{\Psi, \Theta\} = \{\varphi(x), \theta(x)\}\exp(\lambda t + ikz)$$

Substitution of Ψ and Θ into the curl of equations (1) and (2) and neglecting products of perturbation quantities leads to the following system of differential equations for the amplitudes, φ and θ:

$$\lambda\Delta\varphi = \Delta^2\varphi - ik(w_o\Delta\varphi - w_o''\varphi) - R\,Pr^{-1}(ik\sin\alpha\theta + \cos\alpha\theta') \quad (12)$$

$$\lambda\theta = Pr^{-1}\Delta\theta - ik(\theta_o'\varphi + w_o\theta) - \varphi' \quad (13)$$

with the boundary conditions

$$\varphi(\pm 1) = \varphi'(\pm 11) = \theta'(\pm 1) = 0 \quad (14)$$

where

$$\Delta \equiv \frac{\mathrm{d}^2}{\mathrm{d}x^2} - k^2$$

Equations (12)–(14) have nontrivial solutions only for certain values of λ (eigenvalues). The boundary-value problem is not self-adjoint so the eigenvalues λ are in general complex, $\lambda = \lambda_r + i\lambda_i$. The real part λ_r is the rate of damping or amplification of the perturbations and the imaginary part λ_i is the frequency of the oscillations. The results of the stability problem are presented in section 5. The physical interpretation of these results (in section 6) will be performed by considering the energy balance of the perturbations, introduced in the next section.

4. Energy analysis

Physical understanding of the instability mechanisms may be gained by considering the energy balances of equations (12) and (13). By multiplying equation (12) by the complex conjugate of φ, φ^*; multiplying equation (13) by θ^*; integrating from $x = -1$ to $x = 1$ and taking the real part of the resulting equations, the following relationships are obtained:

$$\lambda_r E_m = D_m + M + B_x + B_z, \quad (15)$$

$$\lambda_r E_t = D_t + T_x + T_z, \quad (16)$$

where

$$E_m = \langle|\tilde{u}|^2 + |\tilde{w}|^2\rangle$$

$$D_m = -\langle|\tilde{u}'|^2 + |\tilde{w}'|^2 + k^2(|\tilde{u}|^2 + |\tilde{w}|^2)\rangle$$

$$M = -\langle w_o'\tilde{u}\tilde{w}^*\rangle$$

$$B_x = -R\,Pr^{-1}\sin\alpha\langle\tilde{u}\theta^*\rangle$$

$$B_z = R\,Pr^{-1}\cos\alpha\langle\tilde{w}\theta^*\rangle$$

$$E_t = \langle|\theta|^2\rangle$$

$$D_t = -Pr^{-1}\langle|\theta'|^2 + k^2|\theta|^2\rangle$$

$$T_x = -\langle\theta_o'\tilde{u}\theta^*\rangle$$

$$T_z = \langle\tilde{w}\theta^*\rangle.$$

Brackets stand for the real part of the average in the x direction, i.e., $\langle f\rangle = \mathbf{Re}(\int_{-1}^{1} f(x)\,\mathrm{d}x)$, and

$$\tilde{u}(x) = ik\varphi(x),$$

$$\tilde{w}(x) = -\varphi'(x),$$

are the amplitudes of the cross-stream and axial perturbation velocities.

In equation (15), $\lambda_r E_m$ represents the rate of change of perturbation kinetic energy; D_m the rate of kinetic energy dissipation by viscous forces and M the rate of kinetic energy transfer from the mean flow to the disturbance by momentum advection (energy related to the Reynold stress). The rate at which work is done by buoyancy along x and z axis are respectively, B_x and B_z. Equation (16) represents the balance for the temperature variance (11). $\lambda_r E_t$ is the net rate of change of this quantity, D_t its rate of dissipation by thermal diffusion and T_x, T_z are respectively the advective production of temperature variance due to disturbance motions along x and z directions.

Note that in equation (15) negative terms, as diffusion

($D_m, D_t < 0$) involve a loss of disturbance energy and are thus related to stabilizing effects while, positive terms are related to destabilizing mechanisms. It is possible to anticipate the sign of some kinetic energy terms by physical reasoning. As the fluid is being heated from below, the axial projection of buoyancy tends to amplify any disturbance motion along $z-$axis so, $B_z > 0$. On the other hand, for any $\alpha > 0^\circ$, the mean temperature field has a stable stratification along x (the colder fluid is placed below) so, $B_x < 0$. Finally, note in Fig. 1 that the basic velocity profile has an inflection point at $x = 0$. Due to the occurrence of this inflection point, shear instability modes with $M > 0$ are also expected to appear.

The analysis of the energy contribution of the terms in equations (15) and (16) is simplified by scaling the energy terms with the magnitude of momentum diffusion, $|D_m|$ and temperature diffusion $|D_t|$, respectively. For neutral perturbations, $\lambda_r = 0$, this leads to,

$$1 = m + b_x + b_z. \tag{17}$$

$$1 = t_x + t_z, \tag{18}$$

where $m \equiv M/|D_m|$, $b_i \equiv B_i/|D_m|$ and $t_i \equiv T_i/|D_t|$, with $i = \{x, z\}$.

5. Results

We have solved the characteristic boundary-value problem of equations (12)–(14) by using a Tau–Chebyshev method. The characteristic system of differential equations is reduced to a complex matrix generalized eigenvalue problem, i.e. $(\mathbf{A}-\lambda\mathbf{B})\xi = \mathbf{0}$. The calculations of eigenvalues and eigenvectors were performed using the subroutine EIGZC of the standard IMSL library. The same number of Chebyshev polynomials, N, were used in the stream function and temperature expansions.

The stability of the basic flow in vertical, $\alpha = 0^\circ$ and horizontal $\alpha = 90^\circ$ cavities has been used to validate our results. The calculated values of the critical Rayleigh number and wave number for the onset of convection in vertical cavities, $R^* = 31.28$ and $k_c = 0$, coincide with the analytical result of Gershuni and Zhukhovitskii [6]. Both are independent of Pr as a consequence of the thermal origin of the instability. Our results for the onset of multicellular flow in horizontal cavities have been compared with those corresponding to the transversal shear instability reported in Refs. [9–11]. We obtain the results of Refs. [10 and 11] (e.g. for $Pr = 0.05$, $R_c = 771.97$, $k_c = 1.346$, while in Refs. [10 and 11], $R_c = 771.95$, $k_c = 1.345$). As Laure and Roux pointed out, Hart's [9] results ($R_c = 630$, $k_c = 2.25$ for $Pr = 0.05$) are less accurate because of hardware limitations.

We present results of the stability of the basic flow in inclined cavities in the range of $0^\circ \leqslant \alpha \leqslant 90^\circ$ for $Pr < 0.1$ and for a slightly limited range, $0^\circ \leqslant \alpha < 84^\circ$, for $0.1 \leqslant Pr \leqslant 10$. A typical marginal curve presents two local minima which correspond to different instability branches. In Fig. 3, the values of marginal Rayleigh number are shown vs k, for $Pr = 0.7$, $\alpha = 10^\circ$.

Two different branches are observed: an oscillatory branch which presents a local minima at low values of the wave number and corresponds to rolls of approximately ten times the width of the cavity and a stationary branch with a critical wavelength of nearly two times the width of the cavity. The local minima of the marginal Rayleigh number vs k for the oscillatory and stationary instabilities are respectively denoted by $R_{c,os}$ and $R_{c,st}$ and the corresponding wave number $k_{c,os}$ and $k_{c,st}$. In the case of the oscillatory instability and in the whole range of α and Pr considered, the critical parameters and eigenfunctions calculated with $N = 15$ differed in less than $1/10^4$ with those obtained with larger values of N. For the stationary instability the number of trial functions N needed to ensure the required accuracy increases with α and Pr. For the largest values of Pr and α considered, $N = 24$ were required to obtain deviations less than $1/10^3$. For $Pr > 0.2$, $\alpha > 84^\circ$ and $k > 1.0$ the numerical method does not converge very well and we do not present results for this range. Hart [9] reported the same problem for $Pr > 0.1$ and $\alpha = 90^\circ$ in his numerical method (simple Galerkin in the primitive variable formalism). Laure and Roux [10] and Kuo and Korpela [11] used a Tau–Chebyshev method on the primitive variables formalism but they do not present results of the transversal instability for $Pr > 0.15$ either. Spurious eigenvalues (with no physical meaning) were found. As Brenier et al. [19] pointed out, spurious eigenvalues are likely to be found when using the Tau–Chebyshev method on the stream function and temperature formalism. For $N > 12$, these spurious eigenvalues were easily avoided because they were in all cases at least 10^2–10^3 times greater than the proper ones.

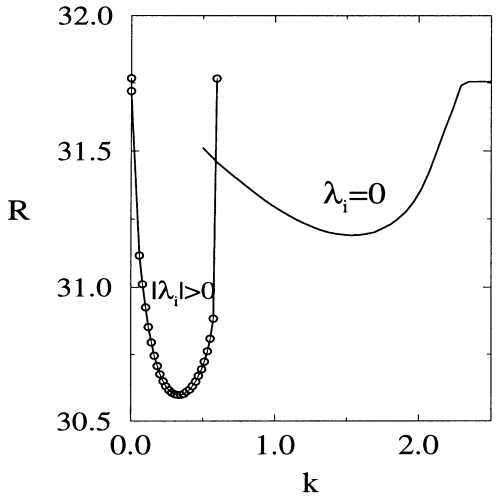

Fig. 3. Neutral stability curve for $Pr = 0.7$ and $\alpha = 10^\circ$.

Table 1
Critical Rayleigh number, wave number and phase velocity, $c = \lambda_i/k$, for the oscillatory instability

	$Pr = 0.3$			$Pr = 0.7$			$Pr = 6.7$		
α	$R_{c,os}$	$k_{c,os}$	c	$R_{c,os}$	$k_{c,os}$	c	$R_{c,os}$	$k_{c,os}$	c
1	31.116	0.183	14.164	31.14	0.213	8.338	31.221	0.138	2.158
10	30.478	0.249	18.524	30.599	0.339	10.341	31.299	0.189	3.190
30	32.988	0.227	27.089	33.092	0.345	14.053	35.213	0.103	6.064
50	42.941	0.175	40.347	42.796	0.303	19.542	47.316	0.061	11.347
70	78.498	0.089	75.167	77.279	0.171	34.347	88.811	0.032	24.921
84	321.83	0.010	457.71	246.44	0.083	102.46	291.65	0.005	99.330

The stability analysis predicts that the oscillatory instability is critical for $Pr < 0.2$, and the stationary instability for $Pr > 0.7$. For intermediate values of the Prandtl number the inclination angle α determines the type of secondary flow.

The dependence of $R_{c,os}$ with α is depicted in Table 1. For any Prandtl number, $R_{c,os}$ grows with the inclination angle roughly like $\sim R^*/\cos\alpha$. $R_{c,st}$ has this same tendency for $Pr > 0.3$ (see Fig. 4a) but for lower Pr it deviates from this trend and decreases with α for $Pr < 0.05$. The dependence of the critical Rayleigh number with Pr is shown in Fig. 5. In the case of the oscillatory instability the effect of Pr depends on the inclination angle: for $\alpha < 30^\circ$, $R_{c,os}$ increase with Pr, while for $\alpha > 30^\circ$ there is first, a slight decrease of $R_{c,os}$ from $0.3 < Pr < 0.7$ and then it rises for larger Pr.

The values of the critical wave number for the stationary instability are shown in Fig. 4b. For $Pr < 0.05$, $k_{c,st}$ is almost independent of the inclination angle (e.g. for

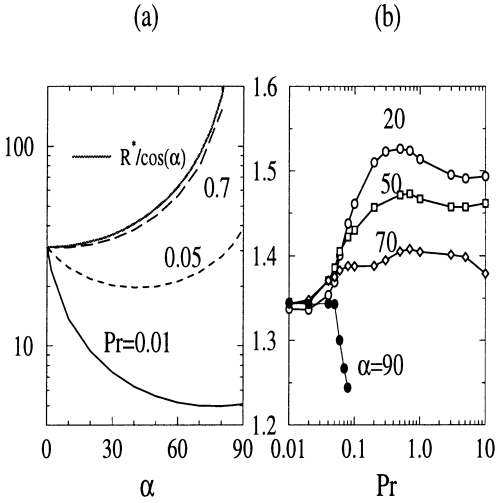

Fig. 4. (a) Critical Rayleigh number ($R_{c,st}$) and, (b) critical wave number ($k_{c,st}$) for the stationary instability.

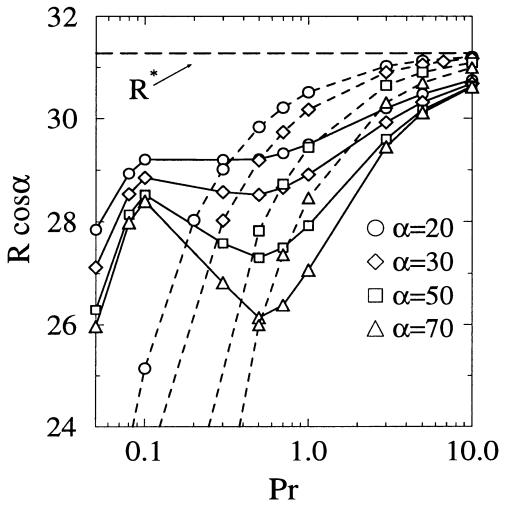

Fig. 5. Axial projection of the critical Rayleigh number vs Pr for several angles. Solid lines correspond to oscillatory and dashed lines to stationary instability.

$Pr < 0.05$, $k_{c,st} \simeq 1.34$, within 2% of variation with α); for larger Prandtl number and $\alpha < 85^\circ$, $k_{c,st}$ increase with Pr and decrease for larger inclinations. The dependence of $k_{c,os}$ with α and Pr is shown in Fig. 6a. The maximum values of $k_{c,os}$ are found at moderate angles (e.g. $k_{c,os} = 0.35$, for $\alpha = 20^\circ$ and $Pr = 0.7$). $k_{c,os}$ falls sharply to zero as $\alpha \to 0$. Concerning the dependence with Pr, the trend of $k_{c,os}$ with Pr reaches a maximum at $Pr = 1$ as Fig. 6b shows.

6. Discussion

6.1. Stationary shear instability

In this section we discuss the behaviour of perturbations with $\lambda_i = 0$. Their energy balance, shown in

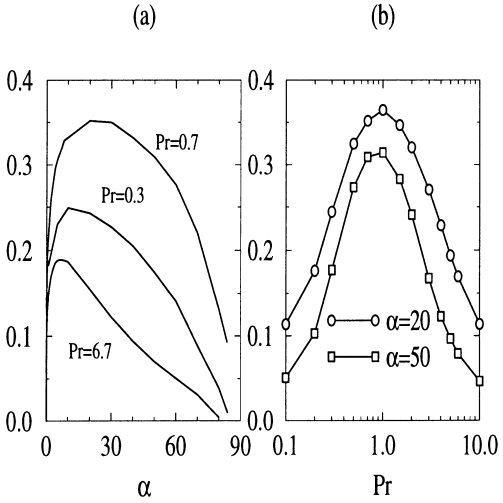

Fig. 6. (a) Critical wave number of oscillatory instability ($k_{c,os}$) vs α and, (b) vs the Prandtl number.

Fig. 7a, reveals that these are shear disturbances in the sense that they obtain most of their kinetic energy from the mean velocity field.

As a consequence of the mechanical origin of the instability, $R_{c,st}$ decreases with Pr and for $Pr < 0.05$ $R_{c,st}$ varies roughly like Pr (see Fig. 5). The corresponding rolls, $k_{c,os}$ are approximately square but have a sizeable dependence on Pr and α which is a consequence of the contribution of the thermal field. This contribution is essentially regulated by the Prandtl number as the energy balance in Fig. 7a shows.

For $Pr \leqslant 0.05$ the kinetic energy released by buoyancy is almost negligible (for instance, $b_x = -0.022$, $b_z = 0.014$, $m = 1.015$, for $Pr = 0.01$). In this range of Pr, $k_{c,os}$ is almost independent of the inclination ($k_{c,st} \approx 1.34$) and the shape of the secondary flow is mainly determined by hydrodynamic effects; i.e., the momentum advection and the momentum diffusion. Fig. 8a shows contours of the perturbation stream function and isotherms for a fluid with $Pr = 0.05$. The energy transfer is primarily from the shear at the center of the layer at $x = 0$, where w'_o maximum.

For Pr above 0.05 another destabilizing mechanism related to the thermal field becomes increasingly important. First, there is a significant rise in the percentage of kinetic energy released by the buoyancy force along z direction (for instance, for $\alpha = 40^\circ$, it grows from 8.5% at $Pr = 0.3$ to 40.4% at $Pr = 10$). Also, for Pr above 0.05, the isotherms of the perturbations tend to be concentrated where the cross-stream advection ($u\theta'_o$) is maximum (note that in the balance of temperature variance, $t_x > 0.91$ for $Pr > 0.2$; see Fig. 7a). These two facts indicate that the destabilizing contribution of buoyancy is, in this case, a consequence of the interplay of the velocity and temperature fields. Consider an up-drift with $u < 0$ generated by shear interaction near $x = 0$. As long as $\theta'_o < 0$, this perturbation carries colder fluid from positive x to the warmer region in $x < 0$. If the cavity were horizontally placed ($\alpha = 90^\circ$), buoyancy would only tend to damp the perturbation owing to the stable mean temperature field. But, in inclined cavities, the upslope buoyancy force can promote motion with $w < 0$ if $R\cos\alpha\theta'$ is large enough. Same reasoning applies where $u > 0$ and $w > 0$. This mechanism favours larger critical wave num-

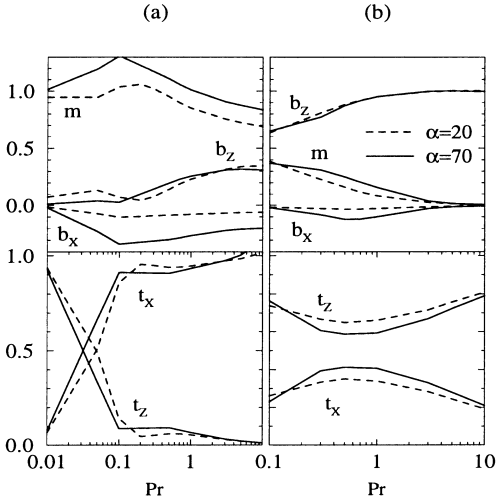

Fig. 7. The energy and temperature variance balances (terms in equations 17 and 18) for (a) stationary and (b) oscillatory critical disturbances.

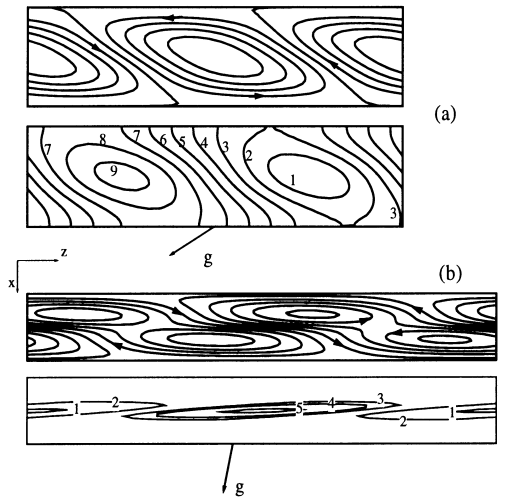

Fig. 8. Contours of stream-function and temperature of critical stationary perturbations for (a) $Pr = 0.05$ and $\alpha = 30$ and (b) $Pr = 10.0$ and $\alpha = 70$.

ber especially at small inclinations (note the increase of $k_{c,st}$ for $Pr > 0.05$ and $\alpha \leqslant 70^\circ$ in Fig. 4b). If this mechanism is not present (as in the case $\alpha = 90^\circ$) the effect of the thermal field for $Pr > 0.05$ is to elongate the shear rolls owing to the rise of thermal stability along x direction. Isotherms and streamlines of a stationary critical perturbation for $Pr = 10$ in an inclined cavity are shown in Fig. 8b.

Finally, note that as $Pr \to \infty$, the mean shear and the temperature stratification needed to put a very viscous fluid into multicellular flow becomes larger and larger, so, $R_{c,st}\cos\alpha$ tends asymptotically to R^* (see Fig. 5).

6.2. Oscillatory thermal instability

The energy balance for the oscillatory disturbances displayed in Fig. 7b, reveals that long-wave oscillatory disturbances are mainly driven by the buoyancy force along z direction.

In vertical cavities, the onset of thermal convection takes place at $R = R^*$ and the critical mode has a vanishing wave number. In the inclined cavity, the values of the critical Rayleigh number, $R_{c,os}$ are close to $R^*/\cos\alpha$ for any Pr as a consequence of the thermal origin of the instability but, on the other hand, secondary flow in the x direction is favoured by two different ways. First, rolls with $k > 0$ take energy out from the mean velocity field (see the energy balance in Fig. 7b). Second, owing to the existence of a mean temperature gradient, particles with cross-stream motions move to new thermal surroundings and experience a buoyancy force in z direction by a mechanism similar to that explained for the shear instability.

The deviations of the critical wave number and Rayleigh number with respect to the corresponding values for the pure conductive state at $\alpha = 0^\circ$ ($k_c = 0$, $R_c = R^*$) may be understood in terms of these two facts. As $Pr \to \infty$ or as $\alpha \to 0^\circ$, the contribution of the mean flow (m) vanishes and the critical modes tend to gain all their energy from the upslope buoyancy so, $k_{c,os} \to 0$ and $R_{c,os}\cos\alpha \to R^*$. On the other hand, both $k_{c,os}$ and t_x present a maximum at $Pr = 1$ (see Figs. 6b and 7b) indicating that the rolls size reduction is also favoured by the coupling of the cross-stream motions and the upslope buoyancy force.

Concerning the dependence on the inclination, for α slightly above zero the damping effect of the cross-stream buoyancy is negligible, and the sharp increase of $k_{c,os}$ with α (see Fig. 6a) indicates the efficiency of the mean flow advection in generating finite rolls. For instance, for $Pr = 0.7$ and $\alpha = 1^\circ$ the size of the thermal rolls are reduced to 8.6 times the width of the cavity. The value of $k_{c,os}$ increases with α until $\alpha \approx 20^\circ$ and decreases for larger inclination owing to the rise in stabilizing cross-stream buoyancy.

The oscillatory disturbance is a standing wave composed of the superposition of a couple of travelling modes carried away by the mean flow with equal and opposite sign phase velocities $\pm\lambda_i/k$. Figure 9 shows contours of the stream function and isotherms of the superposition of the critical travelling waves for $Pr = 0.7$ and $\alpha = 30^\circ$. The critical phase velocity $c \equiv \lambda_i/k$, increases with the inclination angle (see Table 1) according to larger values of the mean flow velocity. For $\alpha \to 0^\circ$ the mean flow vanishes and the associated frequency (λ_i) tends to zero. Another characteristic of this oscillatory instability is that the ratio between c and the maximum mean flow velocity, $w_{o\,\max}$ is independent of the inclination (it varies in less than 1% with α) and only depends on the diffusion properties of the fluid, i.e. on Pr. The phase velocity is lower than $w_{o\,\max}$ and for large Pr, the ratio $c/w_{o\,\max}$ tends to unity (e.g. 0.77, 0.91 respectively for $Pr = 0.7$ and $Pr = 10$).

6.3. Crossover of instabilities

The type of instability that breaks down the unicellular motion is determined by the lowest values of both $R_{c,os}$ and $R_{c,st}$. For infinite cavities, it depends on the Prandtl number and on the inclination angle. The stability boundary in the $\alpha - Pr$ space is shown in Fig. 10. For Prandtl number below to 0.2 stationary shear modes are critical at all angles of inclination while for Pr higher than

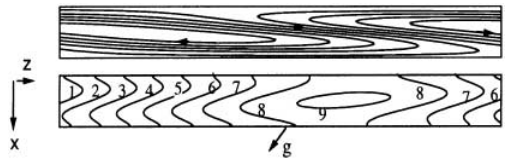

Fig. 9. Contours of stream function and temperature of critical oscillatory perturbations for $Pr = 0.7$ and $\alpha = 30$.

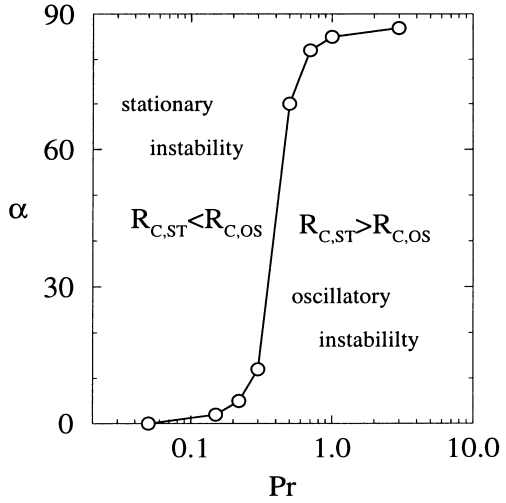

Fig. 10. Stability regions in the Pr–α space.

approximately 0.7, oscillatory thermal modes are critical. In the range $0.2 < Pr < 0.7$, there is an exchange of instability mechanisms at certain angle, α^*. This angle rises steeply near $Pr = 0.5$ revealing a well defined value of the Prandtl number for the onset of stationary or oscillatory disturbances.

7. Numerical solution of the flow in closed geometries

A Chebyshev-collocation pseudospectral method has been used to solve the unsteady two-dimensional Navier–Stokes and heat equations in vorticity-stream function variables for the closed geometry of Fig. 1. The spatial approximation in both directions is based on the expansion of the flow variables in truncated series of Chebyshev polynomials. The time discretization is obtained through an Adam–Bashforth, second order Backward Euler scheme [20]. This is a semi-implicit finite difference scheme; i.e., the diffusive terms are treated implicitly while the non-linear terms are treated explicitly. For each cycle, the equation for the temperature at the next time step consists in a Helmholtz-type equation which is solved by means of a double diagonalization procedure for the algebraic system coming from the Chebyshev collocation method [20]. The corresponding equations for the stream function and vorticity consist of a Stokes-type problem which is solved by using the Influence Matrix technique [20]. This technique avoids the inconvenience of having two boundary conditions for the stream function and none for the vorticity and leads to the solution of several Helmholtz equations with Dirichlet boundary conditions.

According with the results of the linear stability analysis, the calculations have been carried out for several sets of the parameters $(Pr, \alpha, \varepsilon)$ selected to study the onset, evolution and interaction of the stationary oscillatory secondary flow.

In each case, the Rayleigh number was gradually increased to approximately 30% above the critical value. The initial condition was the converged solution for the immediately lower R and the computing time was about $t^* \simeq 10 \times (2h)^2/\nu$. In the unicellular regime the dimensional time step was typically $\Delta t^* \simeq 0.1 \times (2h)^2/\nu$, near the onset of multicellular motion it had to be decreased to $\Delta t^* \simeq 10^{-3}0 \times (2h)^2/\nu$. Some details of the spatial accuracy are given in Table 2, where flow variables as the maximum absolute value of the stream function ($|\Psi|_{MAX}$), the maximum velocity along z and x direction (w_{MAX}, u_{MAX}) and the angular frequency of oscillations (ω) are shown for two different multicellular flow solutions. By using a typical mesh of 33×81 collocation points in the unicellular regime, the flow variables were obtained with accuracies of about 0.1%. For R above the onset of multicellular motion, the number of collocation points was increased to ensure accuracies of about 1%.

To study the oscillatory long-wave thermal rolls, calculations with $Pr = 0.7$, $\alpha = \{20, 50\}$, $\varepsilon = 1/50$ were carried out for increasing R. In both cases the onset of oscillatory multicellular flow occurred abruptly at a certain Rayleigh number. The transition was found at $40 < R \leqslant 45$ and $70 < R \leqslant 75$ respectively for $\alpha = 20$ and $\alpha = 50$, whereas the predicted values of the critical Rayleigh number expressed in terms of the overall temperature gradient are $R_{c,os}/\eta = 44.6$ and $R_{c,os}/\eta = 72.5$. The wave numbers obtained from the numerical solutions of the flow at the onset of the instability ($k = 0.35$ and $k = 0.30$ respectively for $\alpha = 20$ and $\alpha = 50$) are also very close (less than 0.3% of deviation) to those predicted by the stability analysis. In the studied range of R ($R \leqslant 90$, $R \leqslant 60$ respectively for $\alpha = 50, 20$) the flow has an oscillatory behaviour. The numerically calculated angular frequencies, near the onset of the instability (5.46 for $\alpha = 20$ and 7.23 for $\alpha = 50$) are about 20% greater than the linear stability predictions (respectively 4.25, 6.04). In the studied range of R, the fundamental frequency increases almost linearly with R, according to the growth of the mean flow advection. As an example, for $\alpha = 50$, the angular frequency varies from 7.23 at $R = 75$ to 8.46 at $R = 90$.

Calculations with $Pr = 0.7$, $\alpha = \{20, 50\}$ and a smaller $\varepsilon = 1/10$ cavity were performed to investigate the confinement effect. For this set of parameters the critical oscillatory rolls can not develop as their wave number ($k_{c,os} \simeq 0.34$) is smaller than the wave number cutoff imposed by the cavity ($2\pi\varepsilon = 0.628$). Instead, for both $\alpha = 20$ and $\alpha = 50$ a gradual transition to stationary multicellular flow was observed. This fact is illustrated in Fig. 11 where the flow parameter $\delta w_{max} \equiv \mathrm{Max}((1/w_{max})(\partial w_{max}/\partial z))$ is plotted vs R. Note that in the case of $\varepsilon = 1/50$, $\delta w_{max} = 0$ for $R < R_c/\eta$ so the flow at the core is purely parallel below the critical Rayleigh number, but for $\varepsilon = 1/10$, a weak secondary flow exists in the core for $R < R_c/\eta$. The origin of this secondary flow resides on the recirculation eddies developed near the turning regions at the end of the cavity and convected towards the core [18]. For Rayleigh number above the critical one the stationary rolls becomes more and more intense at the core. These results indicate that the fluid undergoes an imperfect bifurcation to multicellular flow induced by the effect of the closing walls. In differentially heated cavities, this type of transition to stationary multicellular flow was first reported by Hart [18] for $\alpha = 90$, $Pr = 0.1$ and $\varepsilon = 1/7$. In horizontal cavities it has been shown [22] that this transition occurs only if $Pr \leqslant 0.12$. Our results show that in inclined cavities the imperfect bifurcation takes place at larger Prandtl number, $Pr \simeq 1$. The explanation of this fact is that, for $\alpha < 90^\circ$ the recirculation eddies are also amplified by the buoyancy force along z direction acting upon the large cross-stream temperature gradient near the turning regions. The wavelength and wave number obtained for

Table 2
Dependence of several flow parameters on the grid mesh. In all cases $\alpha = 20$

ε	R	$N \times M$	$\lvert\Psi_{max}\rvert$	w_{max}	u_{max}	w
0.10	130	31×71	0.181792×10^2	0.298605×10^3	0.137307×10^3	0
0.10	130	33×81	0.182015×10^2	0.301083×10^3	0.138935×10^3	0
0.10	130	33×91	0.181750×10^2	0.300837×10^3	0.139363×10^3	0
0.02	45	31×111	0.159426×10^2	0.124496×10^4	0.562135×10^3	5.53
0.02	45	31×121	0.153550×10^2	0.119442×10^4	0.580461×10^3	5.45
0.02	45	35×131	0.153766×10^2	0.119272×10^4	0.581943×10^3	5.45

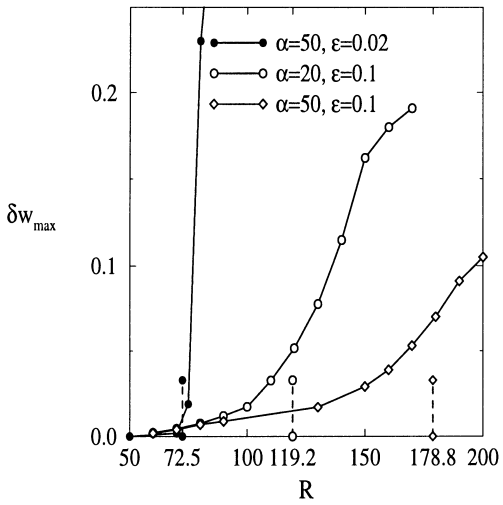

Fig. 11. δw_{max} vs the external Rayleigh number (R). Dashed lines indicate the values of the corresponding critical Rayleigh number predicted by the linear stability analysis, scaled with the external temperature gradient, R_c/η.

$\varepsilon = 1/10$, together with the critical values predicted by the stability analysis are shown in Table 3. Results for several values of R are given to take into account the gradual transition to multicellular motion. For $R \simeq R_c/\eta$, the predicted critical wave number agree in less than 5% but, for increasing R, the stationary rolls become shorter as the recirculation zones near the end regions spread towards the center part of the cavity and reduce the region were the stationary instability develops.

Table 3
Comparison between numerical and critical wave numbers for $Pr = 0.7$ and $\varepsilon = 0.1$; λ is the wavelength

		Numerical		Theoretical
R	α	λ	k	k_c
120	20	4.3 ± 0.2	1.46 ± 0.06	1.52
130	20	4.2 ± 0.3	1.5 ± 0.1	,,
170	50	4.1 ± 0.2	1.5 ± 0.1	1.47
180	50	3.9 ± 0.2	1.6 ± 0.1	,,
190	50	3.7 ± 0.2	1.7 ± 0.1	,,

At $Pr = 0.05$, $\alpha = 10$ and $\varepsilon = 1/30$ the unicellular flow is expected to become multicellular via a transition to stationary shear rolls. According to the linear stability predictions, the flow breaks down at $R_{c,st} = 24.75$ with $k_{c,st} = 1.34$. In the numerical calculations, a set of 11 stationary shear rolls with wave number $k = 1.31$ are observed along the cavity at $25 < R \leqslant 26$. The intensity of the stationary rolls increases with the Rayleigh number until $R = 30$. At this value of R, the stationary pattern evolves to an oscillatory solution with an angular frequency of $\omega = 5.28$. This frequency may be compared with that obtained by Pulicani et al. [21] who found a transition to oscillatory multicellular flow in a cavity with $\varepsilon = 1/4$, $\alpha = 90$ and $Pr = 0.015$ at a (larger) Grashof number ($Gr = R/Pr = 2062$) and an angular frequency $\omega = 23.5$. The second transition to oscillatory flow in low Prandtl fluids is a consequence of mean flow advection [21]. Both frequencies scaled with a time unit characteristic of the mean flow advection, $Gr^{-1}h^2/\nu$, have, in fact, the same order of magnitude ($\omega = 1.1 \times 10^{-2}$ and 0.9×10^{-2} respectively for Ref. [21] and our case).

For $Pr = 0.3$ and $\alpha = 12$ the critical Rayleigh number for stationary and oscillatory transversal instabilities coincides, $R_c = 30.6$. Calculations with this set of parameters and $\varepsilon = 1/60$ were carried out to investigate a transition to a multicellular regime with two types of interacting instabilities. The onset of multicellular motion was found at $35 < R \leqslant 38$ and the corresponding mean local Rayleigh at the core was $30.4 < \eta R \leqslant 31.8$ which is very close to the linear stability prediction. The spatial structure of the flow consisted in fact in the superposition of the two expected types of rolls. A finer mesh of 35×181 collocation points had to be used to correctly solve the flow details. The power spectrum of the stream function along z direction presents two peaks with wave number $k = 0.22$ and $k = 1.51$ which are in good agreement with the predicted critical wave number for oscillatory and stationary instabilities, $k = 0.24$ and $k = 1.53$ respect-

ively. The shear rolls are convected along the cavity, travelling inside the long oscillatory rolls. The flow is oscillatory at $R = 38$. Its fundamental (angular) frequency, 5.17, is close to the frequency of the thermal oscillatory instability, 4.82, obtained in the linear stability analysis.

8. Concluding remarks

The effect of inclined boundaries on the basic and secondary flow in axially heated long finite cavities is the main subject of this paper. The coupling between hydrodynamic and convective mechanisms of instability causes particular properties of the instabilities which arise in the flow. Also, in this simple configuration the instabilities and their interaction can be easily studied by choosing appropriate values of the aspect ratio and inclination angle.

Concerning the basic unicellular flow, we have found that the value of local Rayleigh number at the core region of the cavity is limited by an upper boundary, $R^*/\cos\alpha$.

We have considered the stability of the base flow to transversal perturbations. The results should be valid for cavities with small depth-to-width aspect ratio, where the three dimensional secondary flow is expected to be negligible (see Henkes [13] in the case of horizontal cavities) and two-dimensional perturbations are expected to be critical. A subsequent study will consider longitudinal (three-dimensional) instabilities in a closed geometry.

In two-dimensional inclined cavities, the breakdown of the unicellular flow may be due to shear stationary or thermal oscillatory rolls. The stationary rolls are nearly square and appear for Prandtl below 0.2 while long-wave oscillatory cells of approximately ten times the width of the cavity, appear first for $Pr > 0.7$. For $0.2 < Pr < 0.7$ the critical instability depends on the inclination being oscillatory for low enough tilts. The energy balance of critical perturbations shows that, though stationary and oscillatory perturbations are mainly driven by the mean shear and the upslope buoyancy, for moderate ($\simeq 1$) Prandtl number and non-horizontal tilts the onset of the secondary motion is due to the interplay of both the velocity and thermal fields.

The numerical solution of the flow in the closed geometry has furnished information about the effect of the aspect ratio on the onset of secondary flow. We have found imperfect bifurcations to stationary multicellular flow in an inclined $\varepsilon = 1/10$ cavity, occurring for Prandtl number at least one order of magnitude greater than in the horizontal configuration. Otherwise, in longer cavities, the oscillatory and stationary rolls developed suddenly at Rayleigh number and with wave number quite close to those predicted by the stability analysis.

Acknowledgements

We are indebted to Drs P. Bontoux, J. Ouazzani and B. Brenier for their assistance in the numerical part of the work. We also acknowledge useful discussions with them and Drs M. A. Rubio, and I. Zuñiga. R. Delgado-Buscalioni has been supported by a fellowship from Spanish M.E.C. This work has been supported by DGICYT Projects PB97-0077, PB96-0148 and PB94-382 and A. I. Hispano-Francesa 298B. Computations of Section 7 have been carried out on Cray YMP2E and CRAY C98 computers with support from IMT in Chateau-Gombert, Marseille.

References

[1] P.G. Daniels, P. Wang, On the evolution of thermally driven shallow cavity flows, J. Fluid Mech. 259 (1994) 107.
[2] B.L. Markham, F. Rosenberger, Diffusive–convective vapor transport across horizontal and inclined rectangular enclosures, J. Crystal Growth 67 (1984) 241.
[3] P. Bontoux, C. Smutek, A. Randriamampianina, B. Roux, G.P. Extremet, A.C. Hurford, F. Rosenberger, De Vahl Davis, Numerical solutions and experimental results for three-dimensional buoyancy driven flows in tilted cylinders, in: Adv. Space Res., Pergamon, 1986, p. 155.
[4] A.W. Woods, S.J. Lintz, Natural convection and dispersion in a tilted fracture, J. Fluid Mech. 241 (1992) 59.
[5] P. Cessi, W.R. Young, Fixed-flux convection in a tilted slot, J. Fluid Mech. 237 (1992) 57.
[6] G.Z. Gershuni, E.M. Zhukhovitskii, Convective stability of incompressible fluids, Israel Program for Scientific Translations, Jerusalem, 1976.
[7] D.E. Cormack, L.G. Leal, J. Imberger, Natural convection in a shallow cavity with differentially heated end walls, Part 1. Asymptotic Theory, J. Fluid Mech. 65 (1974) 209.
[8] J. Imberger, Natural convection in a shallow cavity with differentially heated end walls, Part 3. Experimental results, J. Fluid Mech. 65 (1974) 247.
[9] J.E. Hart, A note on the stability of low-Prandtl-number Hadley circulations, J. Fluid Mech. 132 (1983) 271.
[10] P. Laure, B. Roux, Synthèse des résultats obtenus par l'étude de stabilité des mouvements de convection dans une cavité horizontale de grande extension., C.R. Acad. Sci. Paris 305 Série II, (1987) 1137.
[11] H.P. Kuo, S.A. Korpela, Stability and finite amplitude natural convection in a shallow cavity with insulated top and bottom and heated from a side, Phys. Fluids 31 (1) (1988) 33.
[12] R.J.A. Janssen, R.A.W.M. Henkes, Influence of Prandtl number on instability mechanisms and transition in a differentially heated square cavity, J. Fluid. Mech. 290 (1995) 319.
[13] R.J.A. Janssen, R.A.W.M. Henkes, Instabilities in three-dimensional differentially heated cavities with adiabatic horizontal walls, Phys. Fluids 8 (1996) 62.
[14] T. Adachi, J. Mizushima, Stability of thermal convection

in a tilted square cavity, J. Phys. Soc. Jap. 65 (1996) 6, 1686.
[15] E. Crespo del Arco, P. Bontoux, Numerical solution and analysis of asymmetric convection in a vertical cylinder: an effect of Prandtl number, Phys. Fluids A1 (1989) 1348.
[16] J.E. Hart, Stability of the flow in a differentially heated inclined box, J. Fluid Mech. 47 (1971) 547.
[17] A. Bejan, C.L. Tien, Laminar natural convection heat transfer in a horizontal cavity with different end temperatures, J. Heat Transfer 100 (1978) 641.
[18] J.E. Hart, Low Prandtl number convection between differentially heated end walls, Int. J. Heat Mass Transfer 26 (1983) 7.
[19] B. Brenier, B. Roux, P. Bontoux, Comparaison des méthodes Tau–Chebyshev et Galerkin dans l' étude de stabilité des mouvements de convection naturelle. Problème des valeurs propres parasites, J. Mecanique Théorique et Appliquée 5 (1) (1986) 95.
[20] J.M. Vanel, R. Peyret, P. Bontoux, A pseudospectral solution of vorticity-stream function equations using the influence matrix technique, in: K.W. Morton, M.J. Baines, (Eds), Numerical Methods for Fluid Dynamics II, Clarendom Press, Oxford, 1986, pp. 463–475.
[21] J.P. Pulicani, E. Crespo del Arco, A. Randriamampianina, P. Bontoux, Spectral simulation of oscillatory convection at low Prandlt number, Int. J. Number, Meth. Fluids 10 (1990) 481–517.
[22] E. Drummond, S.A. Korpela. Natural convection in a shallow cavity, J. Fluid Mech. 182 (1987) 543.